Annals of Biomedical Engineering, Vol. 40, No. 3, March 2012 *(© 2011)* pp. 606–618
DOI: 10.1007/s10439-011-0423-1

Relationship Between Strain Levels and Permeability of the Plasma Membrane in Statically Stretched Myoblasts

NOA SLOMKA and AMIT GEFEN

Department of Biomedical Engineering, Faculty of Engineering, Tel Aviv University, Tel Aviv 69978, Israel

(Received 8 July 2011; accepted 27 September 2011; published online 7 October 2011)

Associate Editor Eric M. Darling oversaw the review of this article.

Abstract—Deep tissue injury (DTI) is a life-threatening type of pressure ulcer which initiates subdermally with muscle necrosis at weight-bearing anatomical locations, where localized elevated tissue strains exist. Though it has been suggested that excessive sustained soft tissue strains might compromise cell viability, which then initiates the DTI, there is no experimental evidence to describe how specifically such a process might take place. Here, we experimentally test the hypothesis that macroscopic tissue deformations translated to cell-level deformations and in particular, to localized tensile strains in the plasma membrane (PM) of cells, increase the permeability of the PM which could disrupt vital transport processes. In order to determine whether PM permeability changes can occur due to static stretching of cells we measured the uptake of fluorescein isothiocyanate (FITC)-labeled Dextran (molecular weight = 4 kDa) by deformed vs. undeformed myoblasts, using a fluorescence-activated cell sorting (FACS) method. These PM permeability changes were then correlated with tensile strains in the PM which correspond to the levels of substrate tensile strain (STS) that were applied in the experiments. The PM strains were evaluated by means of confocal-microscopy-based cell-specific finite element (FE) modeling. The FACS studies demonstrated a statistically significant rise in the uptake of the FITC-labeled Dextran with increasing STS levels in the STS ≤ 12% domain, which thereby indicates a rise in the permeability of the PM of the myoblasts with the extent of the applied cellular deformation. The cell-specific FE modeling simulating the experiments further demonstrated that applying average PM tensile strains which exceed 3%, or, applying peak PM tensile strains over 9%, substantially increases the permeability of the PM of myoblasts to the Dextran. Moreover, the permeability of the PM grew rapidly with any further increase in PM strains, though there were no significant changes in the uptake above average and peak PM tensile strain values of 9 and 26%, respectively. These results provide an experimental basis for studying the theory that cell-level deformation–diffusion relationships may be involved in determining the tolerance of soft tissues to sustained mechanical loading, as relevant to the etiology of DTI.

Address correspondence to Amit Gefen, Department of Biomedical Engineering, Faculty of Engineering, Tel Aviv University, Tel Aviv 69978, Israel. Electronic mail: gefen@eng.tau.ac.il

Keywords—Cell-specific finite element modeling, Fluorescence-activated cell sorting, Dextran, Deformation-diffusion, Skeletal muscle cells.

ABBREVIATIONS

CSD	Cell stretching device
DTI	Deep tissue injury
FACS	Fluorescence-activated cell sorting
FITC	Fluorescein isothiocyanate
FE	Finite element
GM	Growth medium
PM	Plasma membrane
SED	Strain energy density
STS	Substrate tensile strain
3D	Three-dimensional

INTRODUCTION

Deep tissue injury (DTI) is a life-threatening type of pressure ulcer which initiates with muscle necrosis near a bone–muscle interface and may proceed to spread superficially towards the skin, where it visually debuts in the form of purple or black marks.[1,3,7–9,21,27,44] It is evident that sustained soft tissue deformations play a key role in the etiology of DTI.[15,45] It has further been shown, by means of MRI and patient-specific finite element (FE) modeling, that populations that are known to be at risk for DTI, such as patients with spinal cord injury or post-limb amputation, do exhibit elevated soft tissue strains, particularly large tension strains in skeletal muscle and fat tissues in the susceptible weight-bearing sites.[28,35] Moreover, other FE studies showed that even pure compressive loads delivered at a continuum scale to soft tissues will cause tensional strains at a cell-scale.[40] Hence, studying cellular function under sustained static stretching in living

model systems is particularly relevant to understanding the etiology of DTI.

Using *in vitro* or computer models, it has been suggested by several groups that in individuals with impaired motosensory capacities, the elevated soft tissue strains around bony prominences in the weight-bearing anatomical locations interrupt with normal cell function and eventually lead to cell death.[14,18,41] However, *experimental* evidence for specific cell-scale mechanisms that could cause DTIs is still missing in the literature. In a previous paper, we proposed how macroscopic sustained soft tissue deformations might compromise cell viability, through excessive stretching of the plasma membrane (PM) of the deformed cells which increases PM permeability beyond physiological limits and hence, disrupts normal transport through the PM.[41] If soft tissue loads are relieved intermittently, as in a healthy person who frequently moves while sitting or lying, such temporary PM permeability changes do not produce any clinical symptoms, since the time constants for substantial, detrimental diffusion of biomolecules from the extracellular matrix into the cells or from the cells outwards are longer than the intervals between postural changes. If a person statically maintains his posture for hours, however, as in the case of bedridden or chairfast patients, there is sufficient time for biomolecules that diffuse in a non-controlled manner to build up cytotoxic concentrations intracellularly, or, critical substances may escape the cytosol. This deformation–diffusion mechanism of loss of homeostasis eventually causes cell death, which may later on involve apoptotic reactions as well.[41]

Some supporting evidence for the potential influence of mechanical loads on PM permeability exists in the neurotrauma literature, where several authors reported altered transport through the PM of cultured neurons after subjecting the cells to loading profiles such as instantaneous stretch,[19,20,42] fluid shear stress,[24,25,36] or impact compression.[29] Additional studies consistently provided evidence for mechanically induced PM permeability disruptions in cells subjected to mechanical stress levels exceeding critical thresholds, such as in aortic endothelial cells[17,50] and cardiomyocytes,[23] as well as in alveolar epithelial cells subjected to cyclic stretches.[13,16] Skeletal muscle tissue was the focus of several other studies, investigating stretch-induced muscle damage due to eccentric contractions, particularly in the presence of muscle dystrophies.[2,5,31,47] In this case, the cell-level injury was also proposed to be caused by dynamic stretching of the PM, as demonstrated experimentally in isolated myotubes.[11,37] Nevertheless, the effect of cell-scale static stretching on the permeability of the PM, particularly in the context of the etiology of DTI, has not yet been investigated. Based on the literature reviewed above, we hypothesize that much like dynamic stretch, static sustained cell deformations, as well, are able to increase the PM permeability.

In the present study, we therefore aimed at determining, for the first time, whether and at which PM strain levels does static sustained stretching of skeletal muscle cells (myoblasts), deformed to a physiological extent,[28,35] is able to increase the permeability of the PM.

METHODS

In order to determine whether PM permeability changes occur due to static stretching of the cells, delivered through stretching of the culture substrata, we measured the uptake of fluorescein isothiocyanate (FITC)-labeled Dextran by the deformed vs. undeformed cells, using a fluorescence-activated cell sorting (FACS) method. These PM permeability changes were then correlated with tensile strains in the PM which correspond to the applied levels of substrate stretching. The PM strains were evaluated by means of confocal-microscopy-based three-dimensional (3D) cell-specific FE modeling.[33,38,40] The experimental and modeling procedures are described in detail below.

PM Permeability Studies

Cell Stretching Device

Cells were cultured in six-well culture plates (BioFlex collagen-coated culture plate, Flexcell Inc., NC, USA). The bottom of each well had a 31-mm diameter, 0.51-mm thick flexible, transparent, and collagen-coated culturing substrate, for which we measured the tensile mechanical properties pre-trials using a uniaxial material testing machine (Instron 5544, High Wycombe, UK). We found that at a deformation rate of 5 mm/min the substrate was linearly elastic up to strains of 18% (three repetitions).

A custom-designed cell stretching device (CSD) was built to function in an incubator at standard culturing conditions (temperature of 37 °C, 5% CO_2, and humidity of 90%). To fit in the incubator, the dimensions of the CSD were 20 × 11 × 6 cm and all parts were made of stainless steel 303, excluding the bottom frame which was made of polycarbonate. The CSD allowed to induce controlled radial stretching of the substrata at any desired well (Fig. 1). For this purpose, the six-well culture plate was placed between two rigid frames (Figs. 1a, 1b). Two screws, located at each frame side, allowed the two frames to be brought together gradually at a parallel configuration (Figs. 1a, 1b), which caused controlled stretching of

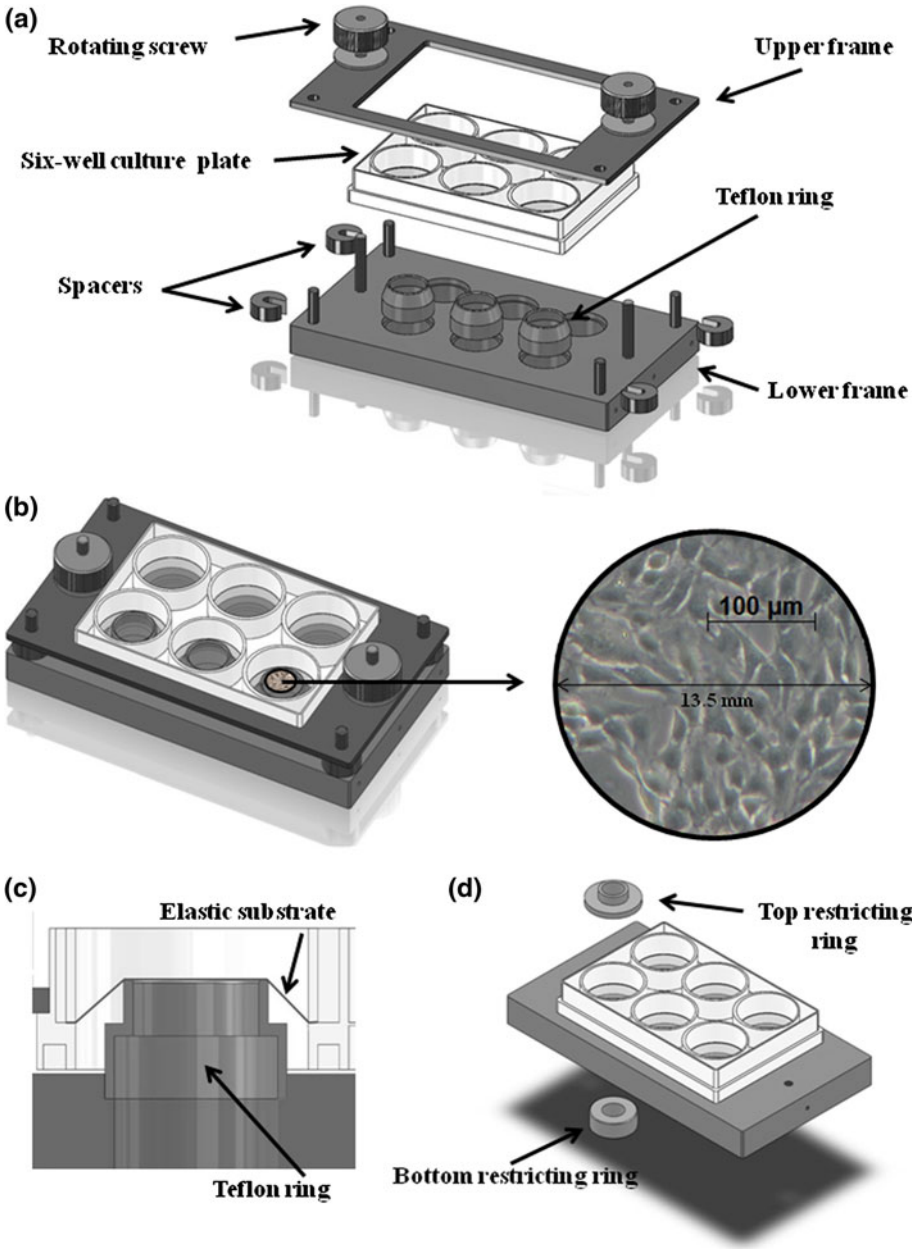

FIGURE 1. The cell stretching device (CSD): (a) The CSD when disassembled. (b) The assembled CSD with the right frame showing cells cultured at the central region of the substrate. (c) The principle of stretching the elastic substrata over Teflon rings that are pushing beneath the substrata. (d) The rings used to restrict cell growth to the central region of the substrata.

substrata in selected wells over Teflon rings positioned underneath the culture plate (Fig. 1c). Four rigid spacers, placed between the frames (Fig. 1a), determined the final distance between the frames. This enabled adequate control over the extent of substrate tensile strains (STSs) following a pre-trial calibration procedure.

To calibrate the STS levels with respect to the distance between the frames of the CSD we marked three ink dots at the center of the substrate and took a series of digital photographs of these marks, first at the undeformed state, and then while gradually lowering the top frame using the screws of the CSD (Fig. 1). Specifically, we lowered the top frame to a distance d from the bottom frame, with d ranging between 1.51 and 0.83 cm at intervals of 0.08 cm ($n = 5$ repetitions per each d value). The finite strain theory was then used in order to calculate the three Eulerian strain components: the circumferential strain (E_{cc}); the radial strain (E_{rr}); and the shear strain (E_{rc}), for each distance between the frames, by means of image processing of the acquired photographs (MATLAB, MathWorks Inc.).[6,26,43]

To verify an equiaxial strain state in the stretched substrata ($E_{cc} = E_{rr}$, $E_{rc} \approx 0$) we further ran a two-factor analysis of variance (ANOVA) for the factors of strain component and distance between the frames d, based on which we calculated the effective tensile strain in the substrata, STS, as the average of E_{cc} and E_{rr} per each d.

Taking together the design constrains of the CSD, the linear elastic domain of the substrate material and the procedure of calibration of the CSD, it was indicated that the STS could be well controlled within a range of 0–12%, at intervals of 3%.

Experimental Design

Undifferentiated C2C12 myoblasts from a murine source (cell line #CRL1722, ATCC, VA, USA) were used in all the experimental procedures reported herein. Cells were maintained undifferentiated in a growth medium (GM) containing Dulbecco's Modified Eagle's medium (with 4.5 g/L glucose, Biological Industries, Beit-Haemek, Israel), 13% fetal bovine serum (Biological Industries), 2 mM L-glutamine (Biological Industries), 0.8% non-essential amino acids (Biological Industries), 1.67% HEPES (Biological Industries), and 50 mg/mL Gentamycin (Biological Industries). Cells were incubated at 37 °C, 5% CO_2 and 90% humidity, and were passaged every 3–4 days upon reaching a confluency of ~80%.[1] The cells used for all experiments were always younger than passage #10. The pH in the media of the cultures, measured using a digital pH meter, was consistently 7.6.

One day prior to stretching, cells were trypsinized and 8×10^4 cells were seeded in each well of the six-well culture plate. Cells in each well were incubated in 1.2 mL of GM. Cell growth was restricted to the central area of the substrate in each well, where the strain field is uniform (see later description of the computational simulations of the experiments). The restriction of culture growth was achieved by placing a custom-made stainless steel 303 ring (inner radius = 13.5 mm) inside each well (Fig. 1d). Rings were also placed below the wells (Fig. 1d) to counteract with the weight of the top rings, so that no mechanical loading was delivered to the cells (by the self-weight of the top rings) at this stage of the experiments. When a confluency of ~80% was achieved in the regions where cultures were allowed to develop (~24 h post-seeding) (see Footnote 1), the restricting rings were removed, and cultures were rinsed with PBS. The culture plate was then immediately placed in the CSD and static stretch levels of 3, 6, 9, or 12% were set for three of the wells. The other three wells were used as non-stretched controls. Cells in all wells were incubated in 5.5 mL GM supplemented with FITC-labeled Dextran (average molecular weight = 4 kDa) (Sigma-Aldrich, Israel) at a concentration of 10^{-4} M[20] for a duration of 3 h. Following this incubation period, substrate stretching was terminated and cells in all wells were kept in their media for additional 10 min as indicated by Geddes and colleagues,[19] who found that in neurons, some stretch-induced PM permeability changes could be repaired 10 min post-delivery of an impact stretch. Cells were then rinsed twice with PBS to remove any extracellular residues of the fluorescent dye, and were then trypsinized and suspended in GM to inhibit the trypsin activity. Next, cells were centrifuged and suspended in 400 μL PBS within flow tubes, which were fed into the FACS analyzer (BDbiosciences, NJ, USA) for determination of the intensity of cell fluorescence. Approximately 5000 cells were scanned per sample using the fluorescence channel (excitation laser 488 nm/em) of the FACS system. The percentage change in fluorescence intensity readings from the stretched cells with respect to readings from the non-stretched controls (from the same trial) was calculated using the Cell Quest software (BDbiosciences). All calculations were corrected for the natural auto-fluorescence of the cells, which was determined through concurrent cultures incubated in GM only.

For the above studies, we subjected three culture triplicates (i.e., $n = 9$) to each STS level. We used a one-factor ANOVA for the factor of the STS level to compare the PM permeability data (quantified by the % change in FITC-Dextran uptake) across the experimental STS conditions. Tukey multiple pairwise comparison tests were used post hoc for comparing the permeability data across STS conditions. A p value lower than 0.05 was considered statistically significant.

We further conducted confocal microscopy studies (Zeiss LSM-510) for visual verification of increased uptake of FITC-labeled Dextran by the stretched cells, where such was detected by the FACS. For this purpose, after conducting the FACS experiments described above, the elastic substrata with the attached cells were gently cut from the stretched as well as from the control wells in preparation for dual morphological fluorescent staining—on top of the incubation with the FITC-labeled Dextran—as follows. Cells were first fixed using 4% paraformaldehyde, and then stained with Rhodamine-labeled Phalloidin (Sigma) to show actin stress fibers. Next, samples were mounted on microscope glass slides using mounting medium fortified with 4′-6-diamidino-2-phenylindole (DAPI) (UltraCruz) to further stain the nuclei of the cells. All confocal images were captured at an objective lens magnification of 40×.

[1] We did not allow cultures to become more confluent than ~ 80% to avoid spontaneous differentiation of myoblasts into myotubes/myofibers.

Simulations of the PM Permeability Studies to Evaluate Corresponding PM Strains

In order to evaluate the tensile strains in the PM as function of the STS levels that were applied in the experimental PM permeability studies we used cell-specific FE modeling.[33,38,40] To allow for variability in PM strains to be estimated as well, we used 3D models of five different randomly selected C2C12 myoblasts. The cell-specific FE modeling methodology is described in detail in the aforementioned publications, and hence, here we review it briefly, for completeness. First, cells which were cultured as described in the previous section were fixed using paraformaldehyde and stained with FITC-labeled Phalloidin (Sigma-Aldrich, Israel). Then, cells were scanned using a confocal microscope (Zeiss LSM-510 microscope) at 0.4 μm intervals along the z-axis, using a 100× magnification lens with a numerical aperture of 1.4 and a pinhole size of 154 μm. Next, the resulted z-stack images were imported to a solid modeling software (SolidWorks 2009, Dassault Systèmes, MA, USA) where contours of the PM and nucleus envelope were delineated at each plane, and per each cell. These contours were lofted to create 3D surfaces describing the cell-specific geometry of each modeled cell. The main geometrical characteristics of each modeled cell are reported in Table 1. The 3D geometry of each cell was then exported to an FE modeling software (ABAQUS version 6.9FE, SIMULIA, RI, USA) for structural, large deformation analyses that will simulate the loading conditions induced in the cells by the CSD. In the FE software, a 10-nm-thick PM was defined for each cell, as the envelope of the cell structure. An elastic substrate was further modeled (separately for each cell), consistent with the experimental configuration (Fig. 2). Modeled cells were located at a random position on their substrata but within a distance of 2/3 the radius of the substrate, as measured from the center of the substrate outwards, to avoid any non-uniformities in the substrate strain field that are associated with boundary effects (see Fig. 2b).

TABLE 1. Geometrical characteristics of the modeled myoblast cells (n = 5).

Geometrical property	Average	SD
Height (μm)	4.1	0.2
Maximal width at base (μm)	54.4	10.8
Area of cell base (μm^2)	1080.2	422.4
Long to short axis ratio at the cell base	2.5	1
Surface area of plasma membrane (μm^2)	2563.4	978.1
Surface area of nucleus (μm^2)	331.4	169
Cellular volume including nucleus (μm^3)	1896.8	847.6
Nuclear volume (μm^3)	113.0	77.5

Parameters were calculated using the solid modeling software "SolidWorks". *SD* stranded deviation.

The PM, cytoplasm, and nucleus were all assumed to be isotropic compressible materials that obey the following Neo-Hookean strain energy density (SED) function[4,10,33,34,38,40]:

$$\mathrm{SED} = \frac{1}{2}k\left(J_3^{1/2} - 1\right)^2 + \frac{1}{2}G\left(J_1 - 3J_3^{1/3}\right) \qquad (1)$$

where $J_1 = \mathrm{tr}(B)$ and $J_3 = \det(B)$ are the first and third invariants of the Finger tensor B, respectively, and k, G are the effective bulk and shear moduli of each cell component. The effective shear moduli assigned to the PM, cytoplasm, and nucleus were adopted from the literature, and were 2.5 kPa,[22] 1.4 kPa,[40] and 2.75 kPa,[12] respectively. Poisson's ratios were taken as 0.45 for all the aforementioned cellular components.[38,40,41]

All cell models were meshed automatically in ABAQUS using the element type M3D6 for the PM and type C3D10M for the cytoplasm and nucleus. The substrate was meshed using the element type C3D15. Numbers of elements ranged between 5024–6112, 20285–30506, 3348–7820 and 15811–16156 for the PM, cytoplasm, nucleus and substrate, respectively, across the different cell models. All material interactions, contact conditions, constraints, and other boundary conditions that applied herein were the same as described in our previous publication concerning cell stretching simulations using cell-specific FE modeling.[38] By quasi-statically displacing the perimeter of the substrate at the radial direction, as occurring in the CSD (Fig. 1c), we were able to analyze the strain distributions in the PM of the individual cell models (Figs. 2, 3). We specifically calculated the average and peak tensile strains occurring in the PM and the area dilatation of the PM for each modeled cell, and the descriptive statistics for these values across all cell models (means and standard deviations) as function of the STS level. All PM strain data are reported here as engineering (Cauchy) strains, which are calculated by ABAQUS from the Green–LaGrange strain values.

RESULTS

The results of the FACS experiments, shown in Fig. 3, demonstrate a statistically significant rise in the uptake of the 4 kDa FITC-labeled Dextran with increasing STS levels in the STS ≤ 12% domain, which thereby indicates a rise in the permeability of the PM of the myoblasts with the extent of the applied cellular deformation. Tukey's post hoc multiple pairwise comparisons showed that the uptake differences between all pairs of STS level conditions were

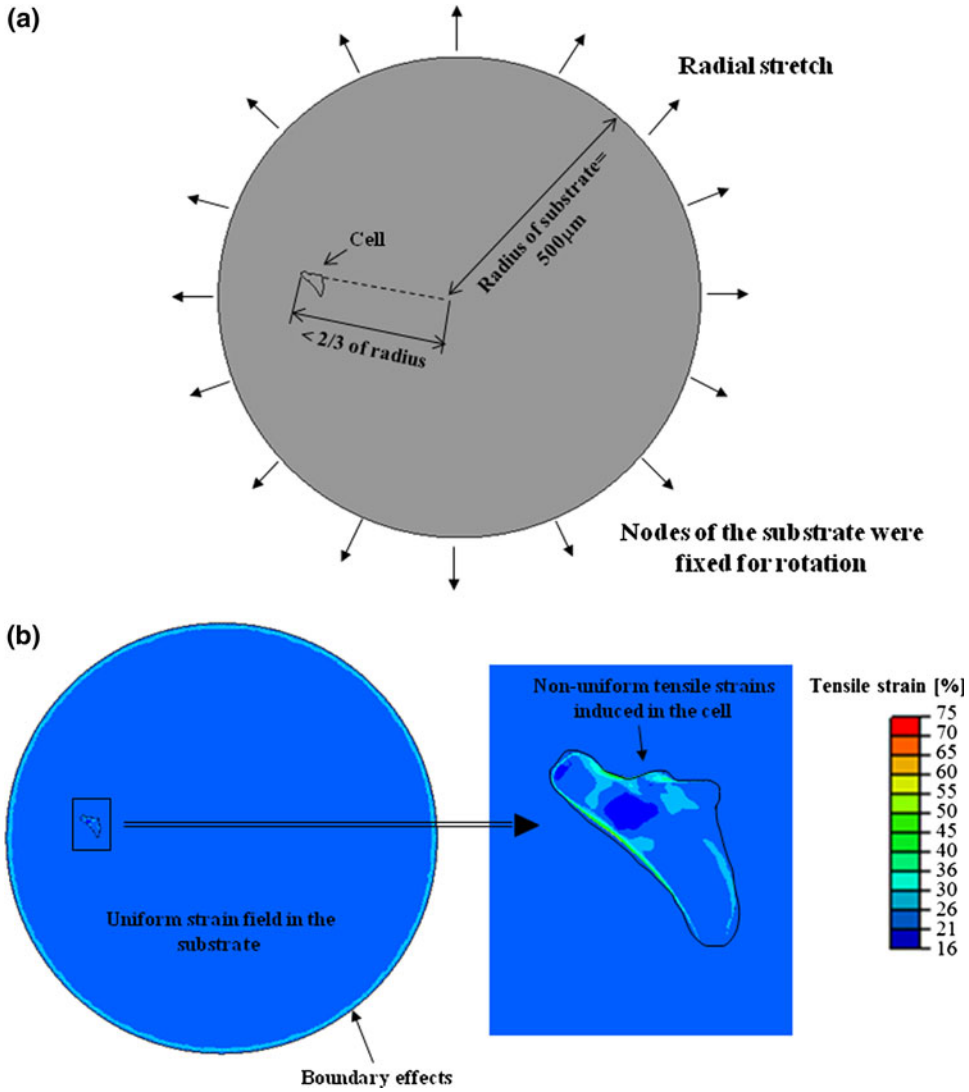

FIGURE 2. Cell-specific finite element modeling of the stretching experiments: (a) Geometry and boundary conditions. (b) An example simulation for cell *A* (see Table 1 for information regarding cell geometry) showing uniformity of tensile strains in the substrate (excluding a ~40-μm-wide marginal zone where boundary effects of the radial displacements occur), as opposed to a non-uniform tensile strain field in the plasma membrane (PM) of the attached cell (magnified in the right frame). This distribution of PM strains corresponds to a simulated substrate tensile strain level of 24%.

statistically significant ($p < 0.05$), excluding the difference between the uptakes at the 9% and 12% STS levels (Fig. 3b). The elevated PM permeability of the stretched cells was also visualized by means of confocal microscopy, which consistently showed negligible uptake of the FITC-labeled Dextran in control (non-stretched) cells as opposed to intensified uptake of the Dextran by the stretched cells (Fig. 4).

The computational simulations of the cell stretching experiments further demonstrated considerably inhomogeneous strain distributions in the PMs, and, in particular, sites of localized tensile strains in the PM of all the five cell models (Fig. 5). The average and peak tensile strains in the PM of the stretched cell models as well as the area dilatation of the PM increased linearly with the STS level (Pearson's correlation coefficient >0.99; Fig. 6), reaching ~12, ~33, and ~26%, respectively, for an STS of 12%.

The Dextran uptake changes measured by the FACS were plotted in Fig. 7 against the PM tensile strains which were calculated using the FE cell models, and which corresponded to the STS levels applied in the experiments. The relationship between Dextran uptake and PM tensile strains takes the form of a sigmoid function (Fig. 7). Specifically, applying average PM tensile strains which exceed 3%, or, applying peak PM tensile strains over 9%, substantially increases the permeability of the PM of myoblasts to

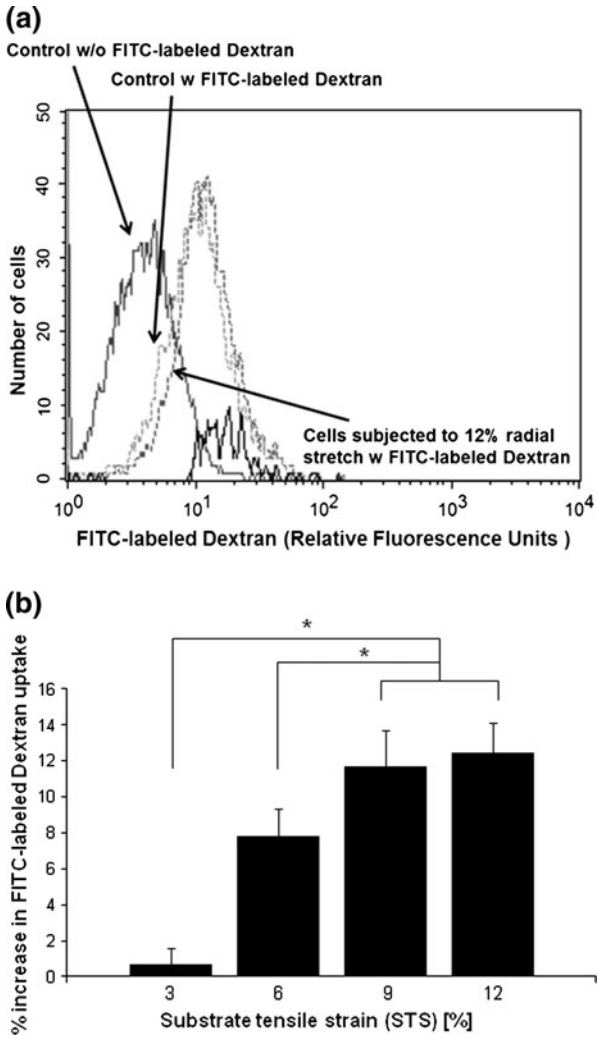

FIGURE 3. Fluorescence-activated cell sorting (FACS) studies: (a) An example of raw fluorescein isothiocyanate (FITC)-labeled Dextran (average molecular weight = 4 kDa) uptake curves obtained from the FACS system for a trial where myoblasts were stretched to a substrate tensile strain (STS) level of 12%. The shift of the curve of the stretched cells demonstrates an increase in their FITC-labeled Dextran uptake with respect to the non-stretched controls. The curve of the signal from the non-stretched and *non-stained* cells is also shown, and is used to correct for natural auto-fluorescence from the cells. (b) The increase in uptake of FITC-labeled Dextran by stretched myoblasts (all data were normalized with respect to non-stretched controls) as a function of the STS, demonstrating the rise in plasma membrane permeability with the extent of cellular deformation. Error bars are standard deviations around the mean value. *p value < 0.05.

4 kDa-sized biomolecules (Fig. 7). Moreover, our results combining the Dextran uptake experiments and cell modeling indicate that the permeability of the PM grows rapidly with any further increase in PM strains beyond the aforementioned levels, though there were no significant changes in the uptake above average and peak PM tensile strain values of 9 and 26%, respectively (Fig. 7).

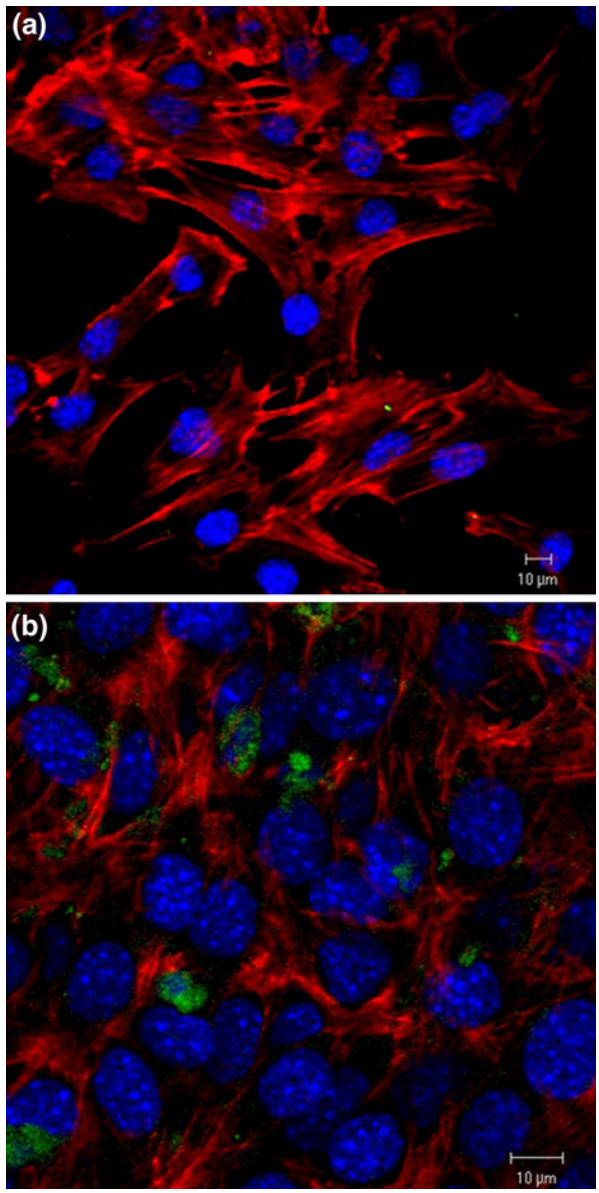

FIGURE 4. Example confocal microscopy images: (a) Myoblasts from a control (non-stretched) culture demonstrating negligible uptake of the fluorescein isothiocyanate (FITC)-labeled Dextran (4 kDa), as evident by minimal green fluorescence. (b) Myoblasts from a culture subjected to substrate tensile strain of 9%, showing intensified uptake of the FITC-labeled Dextran which is manifested as regions of bright green fluorescence (with respect to the control image on top). The morphology of the cells is visualized in the two images using Rhodamine-Phalloidin which stains actin fibers (red) and 4′-6-diamidino-2-phenylindole (DAPI) which stains nuclei (purple).

DISCUSSION

In this study we have quantitatively investigated changes in PM permeability of statically stretched myoblasts as function of the STS and PM strains, by means of FACS analyses coupled with cell-specific FE modeling. Specifically, FACS measurements of 4 kDa

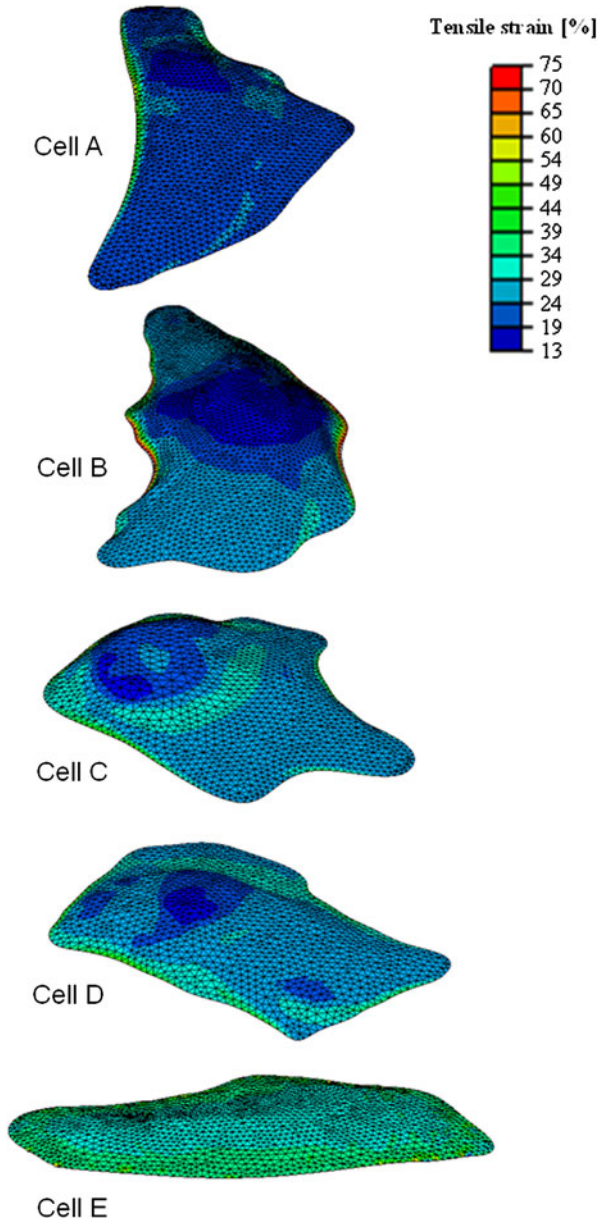

FIGURE 5. Distributions of tensile strains developing in the plasma membrane of all five stretched cell models for a simulated substrate tensile strain of 24%.

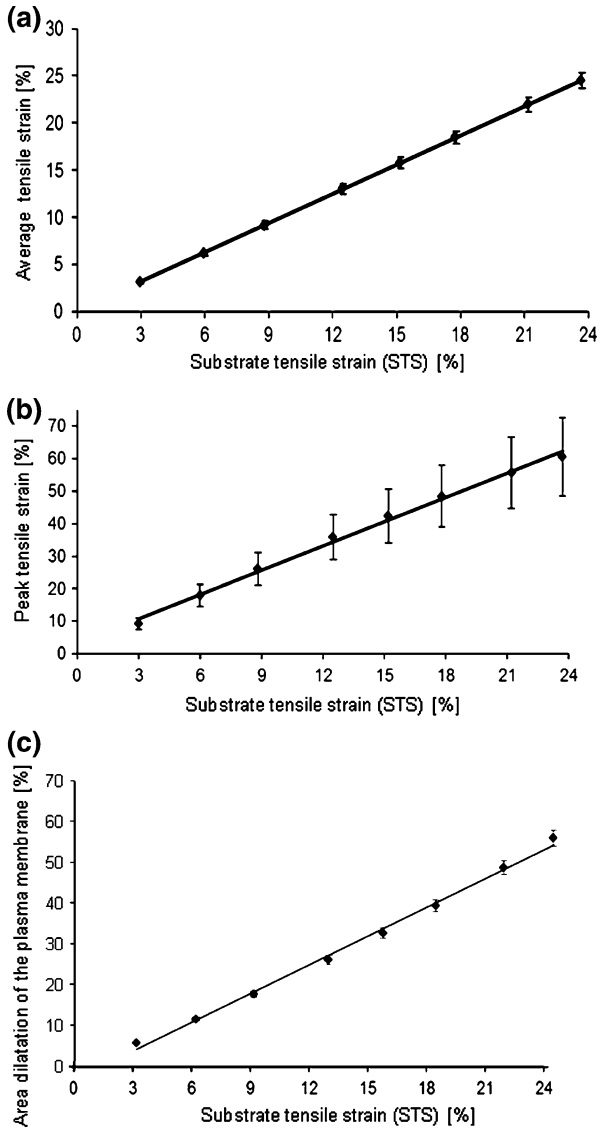

FIGURE 6. Loads in the plasma membrane (PM) of the five cell models as function of the substrate tensile strain level: (a) Average tensile strains in the PM. (b) Peak tensile strains in the PM. (c) Change in surface area of the PM. Error bars are standard deviations around the mean values.

FITC-labeled Dextran uptake by deformed myoblasts (STS between 3 and 12%) with respect to the uptake in control (undeformed) myoblasts were used to demonstrate the increase in PM permeability with the level of stretch of the culture substrate (Fig. 3). By further simulating the experimental configuration using cell-specific FE modeling, the empirically observed PM permeability changes could be correlated with average and peak PM tensile strains of up to approximately 12 and 33%, respectively (Fig. 7).

The area dilatation of the PM is highly relevant in the context of the present work, given that the total uptake of any diffusing biomolecule should rise when the surface areas of the cells increase. It was shown here that the dilatation could exceed 50% for STS levels above 20% (Fig. 6c). The reason for the sharp increase of the PM surface with the STS level is that the area dilatation should theoretically rise approximately proportionally to the square of the substrate stretch ratio (i.e., 1 + STS), as shown analytically in Appendix, where a simplified-geometry model of an attached cell is used to demonstrate this phenomenon. Nevertheless, PM tensile strains, particularly the peak tensile strains should be studied together with the dilatation of the PM, since localized PM deformations

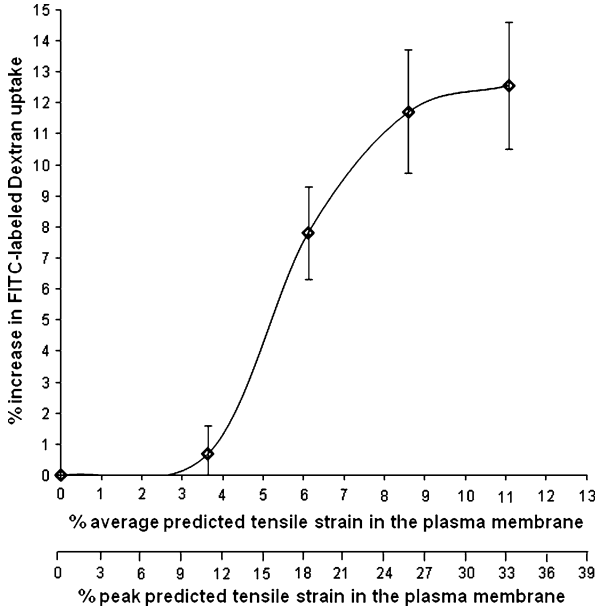

FIGURE 7. The increase in uptake of fluorescein isothiocyanate-labeled Dextran (average molecular weight = 4 kDa) by stretched myoblasts (all data points were normalized to non-stretched controls) as a function of the average and peak tensile strain in the plasma membrane (PM), which were calculated by means of the cell-specific finite element modeling for each substrate tensile strain (STS) level.

may actually be greater than the average PM deformations (Figs. 6a, 6b).

Our finding that there is a trend of increase in PM permeability with the *static* STS levels is in agreement with previous work where a rise in PM permeability was recorded for other cell types in response to *dynamic* mechanical loading.[13,16,19,20] As suggested by these authors when addressing the effects of instantaneous or cyclic loading on PM permeability, it is very likely that in our present experiments, the fluorescent Dextran marker was able to cross the PM barrier through non-specific pores which developed in the PM when cells were distorted. We further surmise, based on the data (Fig. 7), that the numbers and/or sizes of these pores grew with the STS levels, thereby allowing more Dextran to penetrate into the cells when the extent of cellular deformation increased. The minimal size of the defects that apparently appeared in the PM of the stretched cells can be evaluated from the size of the Dextran molecule used in the trials (4 kDa), which has a radius of approximately 1.8 nm,[32] and hence, the typical pores were at least ~3.6 nm wide. Another possible mechanism for the increased PM permeability in the deformed cells, other than uncontrolled separation of the PM, is activation or distortion of mechano-sensitive ion channels.[30,48,49]

Although the confocal studies in Fig. 4 clearly exhibit intensified uptake of Dextran across the stretched cells with respect to non-stretched controls, it is also evident that the extent of uptake of the Dextran dye differs between the stretched cells. The differences in extents of uptake between individual cells are very likely associated with differences in magnitudes of localized PM tensile strains, which in turn depend on the individual cell geometries. Recently, we used cell-specific FE modeling to study the variability across localized tension strains in multiple cells from the same phenotype, myoblasts, and demonstrated variability of up to ~35% in local tension strains in the PM for these cells.[39] In that paper, we further found that the variability in PM strains across cells tends to decay as the deformation of the substrate increases, but for the domain of the STS studied herein (0–12%)—a substantial variability in PM strains across cells should be expected,[39] which is in line with the results of the present confocal microscopy studies that show cell-to-cell differences in uptake of the Dextran dye. To summarize this point, taking our previous work into consideration, we surmise that the cells showing the highest uptake of Dextran at a given substrate tensile strain level were the ones whose geometrical features at the time of stretching caused the highest localized stretching of their PM.

Increasing the STS level from 9 to 12%, or the average PM strains above 9%, or the peak PM strains above 26%, did not result in a further statistically significant increase in PM permeability of the stretched myoblasts in the domain of the substrate and PM strains that were studied herein (Figs. 3b, 7). It is reasonable to expect, however, that this "plateau"-like behavior (Figs. 3b, 7) is local, since theoretically, increasing the STS beyond the levels applied in the present study will eventually cause tears in the PM, which will then allow extracellular biomolecules of any size to flush into the cytosol. It is important to emphasize in this regard that cells in the present study were always viable as evident from routine phase contrast microscopy examinations. The tolerance of the myoblasts to the STS levels that were experimentally applied herein can also be expected theoretically, given that the PM is locally folded and crimped when cells are not externally loaded, hence substrate stretch levels of several-percent-strain are needed just to unfold the natural curvatures of the PM.[46] In other words, when deforming cells by stretching their substrata, elastic energy is first invested in straightening the crimped PM surfaces, and only then do considerable tensile loads start to build up in the PM and be transferred intracellularly. This PM un-crimping process may explain the low-strain portion of the sigmoid function in Fig. 7, below average and peak PM strains of 4 and 12%, respectively, where the increase in the Dextran uptake is negligible to none, since the PM is still fully intact.

Several researchers focused on the effects that dynamic loads have on uptake of extracellular biomolecules by loaded cells, as described in the Introduction section. Dynamic loading is not a scenario which is directly relevant in the clinical context of the present work—DTI. Patients who develop DTI are immobile and typically insensitive, and soft tissue damage in their case is associated with static sustained loads, not dynamic ones. With that being said, pathways for increased PM permeability under dynamic stretching could be different from those involved in static stretching. Viscoelasticity of the PM, in particular, should play a major role in dynamic stretching, where for critical deformation rates the PM could structurally fail, resulting in tears. Experimental data from dynamic and static stretching configurations are therefore not easily comparable.

A few limitations of the present study should be discussed. First, cell-specific FE modeling is more practical to employ for single-nucleated cells (myoblasts in this case) which can be captured in a single field of view of the confocal microscope for geometrical reconstructions, as opposed to myotubes/myofibers. Even if this technical problem can somehow be resolved, the present study is the first to combine cell-specific FE modeling with experimental diffusion studies, and a follow-up study could indeed be focused on multi-nucleated myotubes for which the baseline permeability properties of the PM might be different as well. However, we believe that it is important to understand how individual myoblasts change their permeability under static stretch and at given PM strains before investigating the more complex structure of myotubes/myofibers. Second, fluorescent Dextran is a rather convenient dye to work with, particularly given that it is non-toxic to the cells and can therefore be used for live staining. However, Dextran also has a drawback that it is quite sticky and difficult to remove from the cells, and we therefore cannot rule out completely a possibility that some of the florescence signal detected by the FACS is due to non-specific binding of Dextran to cell surfaces (as opposed to uptake of Dextran by the cells). Hence, one might claim that the area dilatation of the PM, combined with such non-specific binding of Dextran to the PM surfaces caused the observed trend of increase in the fluorescence signal when cells were stretched. However, this is highly unlikely, given that the dilatation increases gradually with the STS, as demonstrated in Fig. 6c (see also the mathematical formulation in Appendix in this regard) but the change in the fluorescence signal does not. In fact, the sharp rise in the fluorescence signal shown between the 3 and 6% STS levels and the almost no change in the signal between the 9 and 12% STS levels point to a threshold behavior, where a critical STS level (or critical tensile strains in the PM; or critical PM dilatation) needs to be exceeded for a mass of Dextran to enter the cells (Fig. 3b). If the fluorescence signal increased merely due to non-specific binding of Dextran to the cell surfaces—the extent of which being increased with the PM dilatation, then a gradual increase in the signal should have been demonstrated, but this is not what the evidence in Fig. 3b or Fig. 7 show. Hence, we conclude that a considerable amount of Dextran must have entered the stretched cells. Third, real-world conditions leading to DTI involve combination of compression, tension and shear strains at the cellular environment, which essentially means that the effects of sustained compression or sustained shearing should also be studied in isolation, using analogue *in vitro* model systems, in order to fully elucidate cellular transport changes in response to sustained loading. As a final point, in the present modeling, we assumed that after applying the stretches to the cells, PM strains remain constant, which implies that the phospholipids profile in the PM is stable and not changing for the duration of the experiments (3 h). This assumption indeed constitutes a limitation to the present modeling, as it is possible that in real-world conditions, the PM might change or adapt its structure over time and thereby—stiffness or strength properties could be altered. Future work, involving investigations of the effects of time on PM permeability is therefore of interest.

In closure, we have shown here that the permeability of the PM grows with increasing levels of sustained tensile strains in the PM of the cells. These findings are in line with our present hypothesis and provide the first experimental support for the proposed roles of cell-level deformation–diffusion relationships in determining tissue tolerance to sustained loading as relevant to the etiology of DTI.[41] Future studies should determine whether the changes in PM permeability observed herein are reversible, and if so, to which extent and after how much time, and most importantly, what is a physiologically "safe" level of PM strain.

APPENDIX: AREA DILATATION IN A SIMPLIFIED-GEOMETRY MODEL OF AN ATTACHED CELL

In order to analytically demonstrate the trend of effect of radial stretching of a substrate on the surface area dilatation of a cell attached to that substrate, consider a simplified-geometry cell model with a disk shape. When the substrate is not stretched and the cell is in its undeformed configuration, the dimensions characterizing the cell are a radius R and a height H.

When the substrate is being stretched to a stretch ratio λ, however (where $\lambda = 1 + \text{STS}$), the cell radius increases to r but due to incompressibility, its height must decrease to h. The volume of this disk-shaped cell, V, should therefore be:

$$V = \pi R^2 H = \pi r^2 h \tag{A1}$$

and the conditions $r > R$ and $h < H$ must be satisfied. Assuming now full attachment of the cell to the substrate, as well as linear elasticity of the substrate material, the radii of the cell at its undeformed and deformed conditions are related by:

$$r = \lambda R \tag{A2}$$

Now substituting Eq. (A2) into Eq. (A1) we obtain:

$$h = H/\lambda^2 \tag{A3}$$

The surface area of the disk-shaped cell at its undeformed configuration, A_u (where A_u also includes the inferior surface of the cell model that faces the substrate) is given by:

$$A_u = 2\pi R^2 + 2\pi RH = 2\pi R(R + H) \tag{A4}$$

Similarly, the surface area of the disk-shaped cell at its deformed configuration, A_d, is given by:

$$A_d = 2\pi r^2 + 2\pi rh = 2\pi r(r + h) \tag{A5}$$

Now we use Eqs. (A2) and (A3) to rewrite Eq. (A5) in terms of the undeformed dimensions of the cell model:

$$A_d = 2\pi\lambda^2 R^2 + 2\pi\lambda r\frac{H}{\lambda^2} = 2\pi R\left(\lambda^2 R + \frac{H}{\lambda}\right) \tag{A6}$$

The surface area dilatation of this simplified-geometry cell can now be calculated as the ratio of cell surface areas in the deformed over the undeformed configurations (A_d/A_u), by diving Eq. (A6) by Eq. (A4):

$$\frac{A_d}{A_u} = \frac{2\pi\lambda^2 R^2 + 2\pi\lambda r\frac{H}{\lambda^2} = 2\pi R\left(\lambda^2 R + \frac{H}{\lambda}\right)}{2\pi R^2 + 2\pi RH = 2\pi R(R + H)} = \frac{\lambda^2 R + \frac{H}{\lambda}}{R + H} \tag{A7}$$

Hence, this first-approximation cell model predicts that for large substrate deformations, the area dilatation should rise proportionally to the square of the substrate stretch ratio.

ACKNOWLEDGMENTS

The authors are thankful to Dr. Uri Zaretsky (Department of Biomedical Engineering at Tel Aviv University) for his help with designing the CSD. We also wish to thank Ms. Naama Shoham (MSc) from the Musculoskeletal Biomechanics Laboratory (Department of Biomedical Engineering at Tel Aviv University) for her assistance with running the CSD calibration process, and Ms. Efrat Leopold from the same lab for helping with the acquisition of the confocal microscopy images. We would further like to thank Ms. Dalit Shav (MSc) and Ms. Riki Levkovitch (MSc) from the Respiratory and Reproductive Bioengineering Laboratory (Department of Biomedical Engineering at Tel Aviv University) for advising us regarding the experimental design. This research is being supported by a grant from the Ministry of Science & Technology, Israel & the Ministry of Research, Taiwan (A.G.).

CONFLICT OF INTEREST

None.

REFERENCES

[1]Agam, L., and A. Gefen. Pressure ulcers and deep tissue injury: a bioengineering perspective. *J. Wound Care*. 16(8):336–342, 2007.
[2]Allen, D. G., N. P. Whitehead, and E. W. Yeung. Mechanisms of stretch-induced muscle damage in normal and dystrophic muscle: role of ionic changes. *J. Physiol.* 567(Pt 3):723–735, 2005.
[3]Ankrom, M. A., R. G. Bennett, S. Sprigle, D. Langemo, J. M. Black, D. R. Berlowitz, and C. H. Lyder. Pressure-related deep tissue injury under intact skin and the current pressure ulcer staging systems. *Adv. Skin Wound Care* 18(1):35–42, 2005.
[4]Baaijens, F. P., W. R. Trickey, T. A. Laursen, and F. Guilak. Large deformation finite element analysis of micropipette aspiration to determine the mechanical properties of the chondrocyte. *Ann. Biomed. Eng.* 33(4): 494–501, 2005.
[5]Bansal, D., K. Miyake, S. S. Vogel, S. Groh, C. C. Chen, R. Williamson, P. L. Mcneil, and K. P. Campbell. Defective membrane repair in dysferlin-deficient muscular dystrophy. *Nature* 423(6936):168–172, 2003.
[6]Barbee, K. A., E. J. Macarak, and L. E. Thibault. Strain measurements in cultured vascular smooth muscle cells subjected to mechanical deformation. *Ann. Biomed. Eng.* 22(1):14–22, 1994.
[7]Black, J. Deep tissue injury: an evolving science. *Ostomy Wound Manage.* 55(2):4, 2009.
[8]Black, J., M. Baharestani, J. Cuddigan, B. Dorner, L. Edsberg, D. Langemo, M. E. Posthauer, C. Ratliff, and G. Taler. National pressure ulcer advisory panel's updated pressure ulcer staging system. *Dermatol. Nurs.* 19(4):343–349, 2007; quiz 350.
[9]Bouten, C. V., C. W. Oomens, F. P. Baaijens, and D. L. Bader. The etiology of pressure ulcers: skin deep or muscle bound? *Arch. Phys. Med. Rehabil.* 84(4):616–619, 2003.
[10]Breuls, R. G., B. G. Sengers, C. W. Oomens, C. V. Bouten, and F. P. Baaijens. Predicting local cell deformations in

engineered tissue constructs: a multilevel finite element approach. *J. Biomech. Eng.* 124(2):198–207, 2002.
[11]Burkholder, T. J. Permeability of C2c12 myotube membranes is influenced by stretch velocity. *Biochem. Biophys. Res. Commun.* 305(2):266–270, 2003.
[12]Caille, N., O. Thoumine, Y. Tardy, and J. J. Meister. Contribution of the nucleus to the mechanical properties of endothelial cells. *J. Biomech.* 35(2):177–187, 2002.
[13]Cavanaugh, K. J., T. S. Cohen, and S. S. Margulies. Stretch increases alveolar epithelial permeability to uncharged micromolecules. *Am. J. Physiol. Cell Physiol.* 290(4): C1179–C1188, 2006.
[14]Ceelen, K. K., C. W. Oomens, A. Stekelenburg, D. L. Bader, and F. P. Baaijens. Changes in intracellular calcium during compression of C2c12 myotubes. *Exp. Mech.* 49:25–33, 2007.
[15]Ceelen, K. K., A. Stekelenburg, S. Loerakker, G. J. Strijkers, D. L. Bader, K. Nicolay, F. P. Baaijens, and C. W. Oomens. Compression-induced damage and internal tissue strains are related. *J. Biomech.* 41(16):3399–3404, 2008.
[16]Fisher, J. L., and S. S. Margulies. Modeling the effect of stretch and plasma membrane tension on Na^+-K^+-Atpase activity in alveolar epithelial cells. *Am. J. Physiol. Lung Cell Mol. Physiol.* 292(1):L40–L53, 2007.
[17]Fung, Y. C., and S. Q. Liu. Elementary mechanics of the endothelium of blood vessels. *J. Biomech. Eng.* 115(1):1–12, 1993.
[18]Gawlitta, D., C. W. Oomens, D. L. Bader, F. P. Baaijens, and C. V. Bouten. Temporal differences in the influence of ischemic factors and deformation on the metabolism of engineered skeletal muscle. *J. Appl. Physiol.* 103(2):464–473, 2007.
[19]Geddes, D. M., R. S. Cargill, II, and M. C. Laplaca. Mechanical stretch to neurons results in a strain rate and magnitude-dependent increase in plasma membrane permeability. *J. Neurotrauma.* 20(10):1039–1049, 2003.
[20]Geddes-Klein, D. M., K. B. Schiffman, and D. F. Meaney. Mechanisms and consequences of neuronal stretch injury in vitro differ with the model of trauma. *J. Neurotrauma.* 23(2):193–204, 2006.
[21]Gefen, A. Bioengineering models of deep tissue injury. *Adv. Skin Wound Care* 21(1):30–36, 2008.
[22]Hochmuth, R. M., N. Mohandas, and P. L. Blackshear, Jr. Measurement of the elastic modulus for red cell membrane using a fluid mechanical technique. *Biophys. J.* 13(8):747–762, 1973.
[23]Kaye, D., D. Pimental, S. Prasad, T. Maki, H. J. Berger, P. L. Mcneil, T. W. Smith, and R. A. Kelly. Role of transiently altered sarcolemmal membrane permeability and basic fibroblast growth factor release in the hypertrophic response of adult rat ventricular myocytes to increased mechanical activity in vitro. *J. Clin. Invest.* 97(2):281–291, 1996.
[24]Laplaca, M. C., V. M. Lee, and L. E. Thibault. An in vitro model of traumatic neuronal injury: loading rate-dependent changes in acute cytosolic calcium and lactate dehydrogenase release. *J. Neurotrauma* 14(6):355–368, 1997.
[25]Laplaca, M. C., and L. E. Thibault. An in vitro traumatic injury model to examine the response of neurons to a hydrodynamically-induced deformation. *Ann. Biomed. Eng.* 25(4):665–677, 1997.
[26]Lee, A. A., T. Delhaas, L. K. Waldman, D. A. Mackenna, F. J. Villarreal, and A. D. Mcculloch. An equibiaxial strain system for cultured cells. *Am. J. Physiol.* 271(4 Pt 1): C1400–C1408, 1996.
[27]Linder-Ganz, E., and A. Gefen. Stress analyses coupled with damage laws to determine biomechanical risk factors for deep tissue injury during sitting. *J. Biomech. Eng.* 131(1):011003, 2009.
[28]Linder-Ganz, E., N. Shabshin, Y. Itzchak, Z. Yizhar, I. Siev-Ner, and A. Gefen. Strains and stresses in sub-dermal tissues of the buttocks are greater in paraplegics than in healthy during sitting. *J. Biomech.* 41(3):567–580, 2008.
[29]Luo, J., R. Borgens, and R. Shi. Polyethylene glycol immediately repairs neuronal membranes and inhibits free radical production after acute spinal cord injury. *J. Neurochem.* 83(2):471–480, 2002.
[30]Mcbride, T. A., B. W. Stockert, F. A. Gorin, and R. C. Carlsen. Stretch-activated ion channels contribute to membrane depolarization after eccentric contractions. *J. Appl. Physiol.* 88(1):91–101, 2000.
[31]Mcneil, P. L., and R. Khakee. Disruptions of muscle fiber plasma membranes. Role in exercise-induced damage. *Am. J. Pathol.* 140(5):1097–1109, 1992.
[32]Oliver, J. D., III, S. Anderson, J. L. Troy, B. M. Brenner, and W. H. Deen. Determination of glomerular size-selectivity in the normal rat with Ficoll. *J. Am. Soc. Nephrol.* 3(2):214–228, 1992.
[33]Or-Tzadikario, S., and A. Gefen. Confocal-based cell-specific finite element modeling extended to study variable cell shapes and intracellular structures: the example of the adipocyte. *J. Biomech.* 44(3):567–573, 2010.
[34]Peeters, E. A., C. W. Oomens, C. V. Bouten, D. L. Bader, and F. P. Baaijens. Mechanical and failure properties of single attached cells under compression. *J. Biomech.* 38(8):1685–1693, 2005.
[35]Portnoy, S., I. Siev-Ner, N. Shabshin, A. Kristal, Z. Yizhar, and A. Gefen. Patient-specific analyses of deep tissue loads post transtibial amputation in residual limbs of multiple prosthetic users. *J. Biomech.* 42(16):2686–2693, 2009.
[36]Prado, G. R., J. D. Ross, S. P. Deweerth, and M. C. Laplaca. Mechanical trauma induces immediate changes in neuronal network activity. *J. Neural. Eng.* 2(4):148–158, 2005.
[37]Sampaolesi, M., T. Yoshida, Y. Iwata, H. Hanada, and M. Shigekawa. Stretch-induced cell damage in sarcoglycan-deficient myotubes. *Pflugers Arch.* 442(2):161–170, 2001.
[38]Slomka, N., and A. Gefen. Confocal microscopy-based three-dimensional cell-specific modeling for large deformation analyses in cellular mechanics. *J. Biomech.* 43(9): 1806–1816, 2010.
[39]Slomka, N., and A. Gefen. Cell-to-cell variability in deformations across compressed myoblasts. *J. Biomech. Eng.* 133:081007, 2011.
[40]Slomka, N., C. W. J. Oomens, and A. Gefen. Evaluating the effective shear modulus of the cytoplasm in cultured myoblasts subjected to compression using an inverse finite element method. *J. Mech. Behav. Biomed. Mater.* 4:1559–1566, 2011.
[41]Slomka, N., S. Or-Tzadikario, D. Sassun, and A. Gefen. Membrane-stretch-induced cell death in deep tissue injury: computer model studies. *Cell Mol. Bioeng.* 2:118–132, 2009.
[42]Smith, D. H., J. A. Wolf, T. A. Lusardi, V. M. Lee, and D. F. Meaney. High tolerance and delayed elastic response of cultured axons to dynamic stretch injury. *J. Neurosci.* 19(11):4263–4269, 1999.
[43]Sotoudeh, M., S. Jalali, S. Usami, J. Y. Shyy, and S. Chien. A strain device imposing dynamic and uniform equi-biaxial

strain to cultured cells. *Ann. Biomed. Eng.* 26(2):181–189, 1998.

[44]Stekelenburg, A., D. Gawlitta, D. L. Bader, and C. W. Oomens. Deep tissue injury: how deep is our understanding? *Arch. Phys. Med. Rehabil.* 89(7):1410–1413, 2008.

[45]Stekelenburg, A., C. W. Oomens, G. J. Strijkers, K. Nicolay, and D. L. Bader. Compression-induced deep tissue injury examined with magnetic resonance imaging and histology. *J. Appl. Physiol.* 100(6):1946–1954, 2006.

[46]Vlahakis, N. E., M. A. Schroeder, R. E. Pagano, and R. D. Hubmayr. Role of deformation-induced lipid trafficking in the prevention of plasma membrane stress failure. *Am. J. Respir. Crit. Care Med.* 166(9):1282–1289, 2002.

[47]Whitehead, N. P., M. Streamer, L. I. Lusambili, F. Sachs, and D. G. Allen. Streptomycin reduces stretch-induced membrane permeability in muscles from Mdx mice. *Neuromuscul. Disord.* 16(12):845–854, 2006.

[48]Yeung, E. W., and D. G. Allen. Stretch-activated channels in stretch-induced muscle damage: role in muscular dystrophy. *Clin. Exp. Pharmacol. Physiol.* 31(8):551–556, 2004.

[49]Youm, J. B., J. Han, N. Kim, Y. H. Zhang, E. Kim, H. Joo, C. Hun Leem, S. Joon Kim, K. A. Cha, and Y. E. Earm. Role of stretch-activated channels on the stretch-induced changes of rat atrial myocytes. *Prog. Biophys. Mol. Biol.* 90(1–3):186–206, 2006.

[50]Yu, Q. C., and P. L. Mcneil. Transient disruptions of aortic endothelial cell plasma membranes. *Am. J. Pathol.* 141(6): 1349–1360, 1992.